PIER C

Linear-to-Circular Polarization Conversion Metasurfaces with Multibeam for Ka-Band Satellite Applications

Jinfeng He, Honggang Hao*, Ting Zhang, Dan Yin, and Zhilin Zou

School of Optoelectronic Engineering, Chongqing University of Posts and Telecommunications, Chongqing, China

ABSTRACT: In this paper, a transmissive linear-to-circular polarization conversion (LCPC) multibeam metasurface is presented which shows promise for point-to-multipoint transmission in satellite communications under interference conditions. The unit cell consists of four identical metal layers and three dielectric substrates, where each metal layer includes a square ring and a cross-shaped structure. By altering the arm length of the cross-shaped structure, independent control of the phase of x- and y-polarized waves can be achieved. Thus, by keeping the amplitude of the x- and y-polarized waves equal and the phase difference at $90°$, LCPC is realized. Based on the multibeam superposition theorem, the metasurface array is arranged using four discrete elements with a phase gradient of $90°$. It can convert linearly polarized (LP) waves into right-handed circularly polarized (RHCP) waves and generate transmitted multibeam at predetermined angles and gain ratios. Three-beam LCPC metasurfaces with equal and unequal gain in the Ka-band (26 to 40 GHz) were demonstrated to validate the proposed unit cell and methods. The equal gain metasurface has an approximate 6% bandwidth for the 3 dB axial ratio (AR) and a 6% bandwidth for the 1 dB realized gain. Furthermore, at the center frequency of 30 GHz, the unequal gain metasurface achieves gains of 22.9 dBi, 19.7 dBi, and 17.3 dBi, respectively, with an AR of less than 2 dB for all three beams.

1. INTRODUCTION

Satellite communication is a technology that uses artificial satellites as relay stations to transmit electromagnetic waves, providing global connectivity and high-rate communication in the high-frequency band. It is vital for disaster relief and military communication due to its reliability and wide coverage [1]. However, polarization mismatches between reception and transmission [2] and a lack of spectrum resources [3] for LP waves in satellite communication systems create significant challenges to antenna technology. The frequency bands for satellite communication primarily include C-band, Ku-band, and Ka-band [4], which are widely employed in various types of satellite communication systems, resulting in spectrum exhaustion. To improve the communication system's spectrum utilization efficiency and data transmission rate, researchers borrowed the multi-access linking method of satellite communication and adopted multi-beam [5] technology to enable parallel communication between satellites and multiple ground stations or user terminals. LP waves will suffer from the Faraday rotation effect after passing through the ionosphere, resulting in polarization angle deflection and reduced polarization matching between transmitter and receiver; however, circularly polarized (CP) waves remain co-rotating after being deflected by the ionosphere [6]. Thus, choosing circularly polarized waves for propagation in satellite communication can improve signal transmission quality and stability while enhancing the communication system's anti-interference ability.

Metasurfaces [7] are two-dimensional metamaterials with flexible control, consisting of meta-atoms with specific shapes, sizes, and arrangements. The electromagnetic properties of incident waves, such as amplitude, phase, and polarization, can be regulated by adjusting the structure of the unit. The multibeam forming of metasurfaces offers the advantages of compactness, flexibility, low cost, and efficiency. In 2019, Bao et al. [8] proposed a C-shaped reflective metasurface with simultaneous amplitude and phase modulation capability, which utilized the principle of complex reflection coefficient superposition to generate multibeams with adjustable amplitude and phase. Sun et al. [9] presented a wide-angle Huygens metasurface to enhance the gain of multiple beams based on the Huygens principle. In the last few years, several monolayer or multilayer LCPC metasurfaces have been proposed [10, 11] to get a certain 3 dB AR bandwidth and conversion efficiency. However, their research only deals with the case of single-beam vertical transmission, while for CP multibeam metasurfaces, Yang et al. [12] used three microstrip patch antennas as feed sources to provide incident waves in three different directions and then achieved a circularly polarized transmissive three-beam. The cost and design complexity of the way to generate multi-beam by using multiple feeds are high. Jiang et al. [13] generated CP multi-beam by employing a single-horn feed with a Berry Phase Transmit Array (BPTA). Based on this, a metasurface array capable of producing unequal gain CP four beams is designed and fabricated by using the intersection approach for pattern synthesis, which can be applied to point-to-multipoint satellite communications. So LCPC multi-beam metasurfaces with adjustable gain ratios can be used to decrease multipath fading and atmospheric effects in satellite communications.

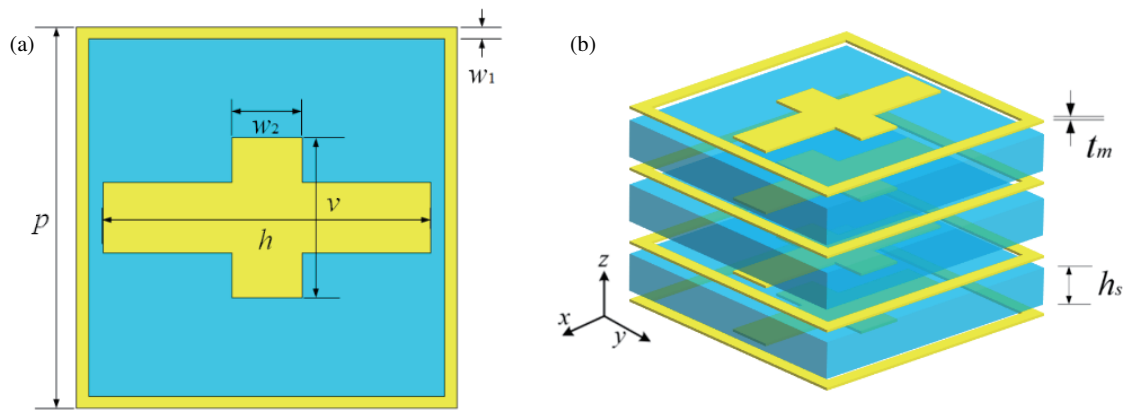* Corresponding author: Honggang Hao (haohg@cqupt.edu.cn).

FIGURE 1. Schematic diagram of unit cell. (a) Top view of unit. (b) 3D view of the unit.

In this paper, a transmissive LCPC multibeam metasurface in the Ka-band is proposed. The metasurface unit consists of a metallic square ring and a cross-shaped structure with a period of $0.31\lambda_0$ (λ_0 is the wavelength in free space at the center frequency of 30 GHz), and the dimension of the metasurface array is $124\,\text{mm} \times 124\,\text{mm} \times 2.54\,\text{mm}$. The x- and y-polarized waves are independently controlled by changing the arm-length size of the cross-shaped structure to achieve multi-beams of equal and unequal gain. The results show that the proposed metasurface has high gain and good LCPC performance, which can improve spectrum utilization and is available for point-to-multipoint transmission in satellite communications.

2. DESIGN AND SIMULATION OF UNIT CELL

As known to all when an LP electromagnetic wave is incident along the 45° direction, the incident electric field $\vec{E}_i$ can be decomposed into:

$$\vec{E}_i = E_x\hat{a}_x + E_y\hat{a}_y \qquad (1)$$

where E_x and E_y are the electric field components in the x- and y-directions, respectively, and their corresponding transmission coefficients are T_{xx}, T_{yx}, T_{yy}, and T_{xy}. For the design of the cross-shaped structure, the effect of cross-polarization is negligible, i.e., $T_{yx} = T_{xy} = 0$. In this case, the transmitted electric field $\vec{E}_t$ can be expressed as follows:

$$\vec{E}_t = T_{xx}E_x\hat{a}_x + T_{yy}E_y\hat{a}_y \qquad (2)$$

When $|T_{xx}| = |T_{yy}|$ and $\Delta\varphi = \arg(T_{xx}) - \arg(T_{yy}) = \varphi_{xx} - \varphi_{yy} = \pm\pi/2$, the transmitted wave is a circularly polarized wave where "$\pi/2$" is taken as a right-handed circularly polarized wave and "$-\pi/2$" as a left-handed circularly polarized wave.

As illustrated in Fig. 1, the unit cell is made up of four identical metal layers and three dielectric substrates, with dielectric substrate material F4B ($\varepsilon_r = 2.65$, $\tan\delta = 0.001$) having a thickness of $h_s = 0.8\,\text{mm}$. Fig. 1(a) shows that the top metal patch is composed of a square ring and a cross-shaped structure with a unit period of p. The width of the metal square ring is w_1; the width of the cross-shaped structure is w_2; and the cross arm length and longitudinal arm length are set to the variables h and v with the following dimensional parameters: $p = 3.1\,\text{mm}$, $w_1 = 0.1\,\text{mm}$, $w_2 = 0.57\,\text{mm}$, $h_s = 0.8\,\text{mm}$, and $t_m = 0.035\,\text{mm}$.

The unit is modeled and simulated using the electromagnetic simulation software CST, with the x- and y-directions set as periodic boundary conditions, the z-direction set as open (add space), and the port set as a Floquet port for generating x- and y-polarized waves, respectively. Fig. 2 shows the surface current and electric field distributions at the center frequency of 30 GHz. When x- and y-polarized waves are incident, the major currents along the x and y axes are produced. The electric field distribution reveals that the resonance occurs mostly in the direction of the incident wave's polarization. As a result, the electric fields of x- and y-polarized waves can be independently regulated by varying the lengths of the transverse arm, h, and the longitudinal arm, v, respectively, that is, changing h only affects the transmitted phase of the x-polarized incident wave, while changing v only affects the transmitted phase of the y-polarized incident wave.

Figure 3(a) shows the curves of the co-polarized transmission amplitude and phase of the unit cell varying with the parameter h when the incident wave is x-polarized, while Fig. 3(b) displays the corresponding curves when the incident wave is y-polarized, varying with the parameter v. It reveals that adjusting the cross arm length and longitudinal arm length of the cross-shaped structure allows the unit to have different phase and amplitude responses for incident waves of various polarization directions. The proposed unit has central symmetry, so the co-polarized transmission phase and amplitude responses for x-polarization and y-polarization are essentially the same. Both satisfy the phase coverage of 0–350°, and the transmission amplitude is more than 0.8.

In order to realize the LCPC, $|T_{xx}| = |T_{yy}|$ and $\Delta\varphi = \arg(T_{xx}) - \arg(T_{yy}) = \varphi_{xx} - \varphi_{yy} = \pm\pi/2$ should be satisfied, i.e., four cells with the co-polarized transmittance phase difference of 90° and equal transmittance amplitude for x-polarization and y-polarization are selected as the alternative cells for array deployment. The arm length dimensions and corresponding co-polarized amplitude/phase of the selected four cells are listed in Table 1, and the structure of the four cells is shown schematically in Fig. 4.
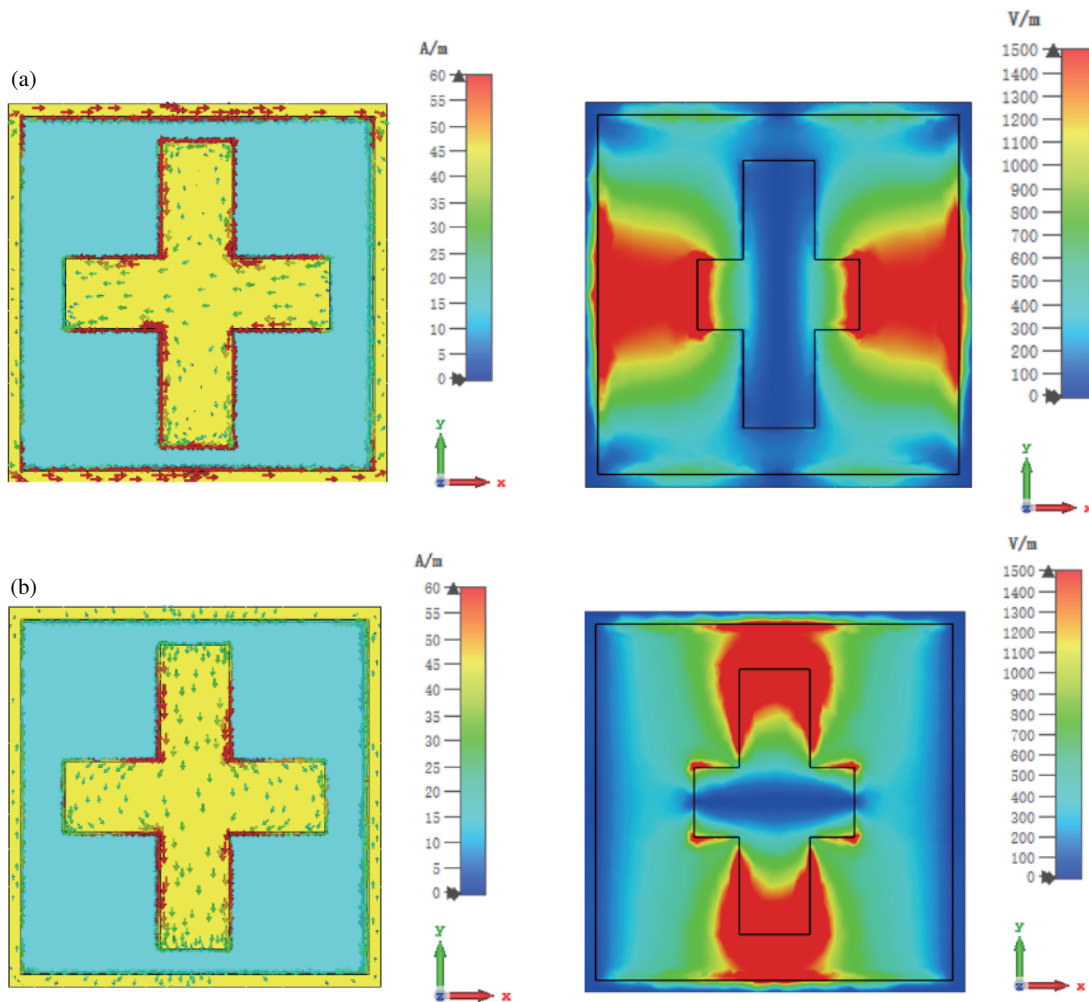
FIGURE 2. Surface current and electric field distribution of the unit cell. (a) The incident wave is x-polarized. (b) The incident wave is y-polarized.
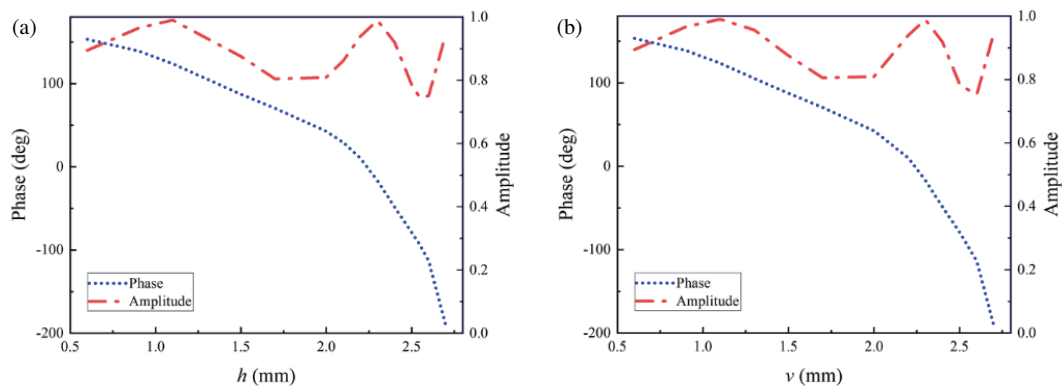

FIGURE 3. Co-polarized transmission amplitude and phase of the unit cell. (a) The x-polarized wave varies with h. (b) The y-polarized wave varies with v.

The simulation analysis of the co-polarized amplitude and phase of the four cells under the incidence of orthogonal LP waves is carried out in the frequency range of 26–34 GHz in the Ka-band. The co-polarized transmission phase gradient of the x/y polarization of any two adjacent cells is approximately 90°, as shown in Fig. 5. Additionally, each cell's x- and y-

polarization phase differences are also 90°, and all transmission amplitudes are greater than 0.85 at the center frequency of 30 GHz. It is known that an arbitrary CP wave can be decomposed into two orthogonal LP waves, x-polarization and y-polarization, with a phase difference of 90°. Hence, the incident LP wave can be transformed into a CP wave by main-
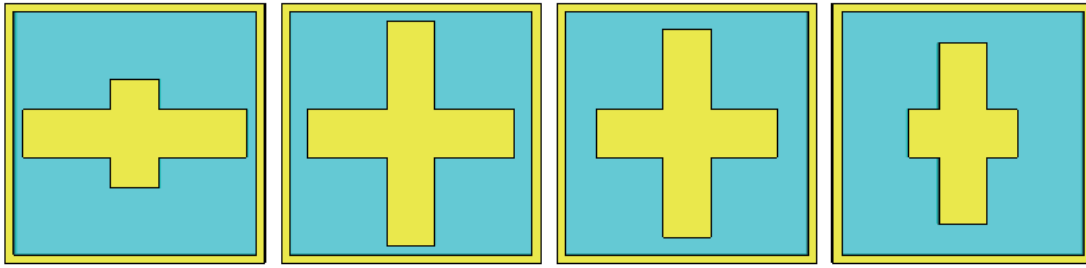
FIGURE 4. Schematic diagram of the four selected unit cells.

TABLE 1. Arm length dimensions and co-polarized amplitudes and phases of the selected unit cells.

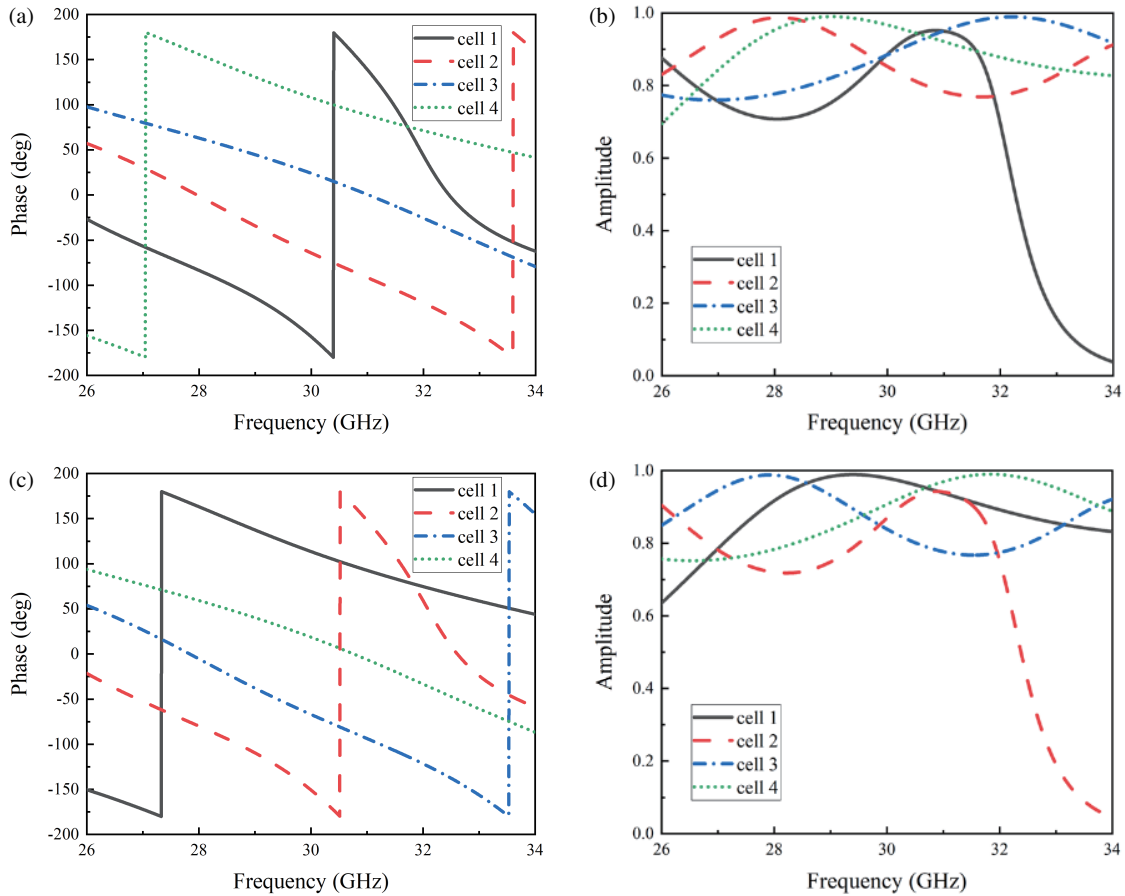| cell	1	2	3	4
h (mm)	2.67	2.48	2.16	1.3
v (mm)	1.3	2.67	2.48	2.16
T_{xx}	0.892	0.852	0.884	0.967
φ_{xx} (°)	-159.3	-64.3	24.3	107.9
T_{yy}	0.979	0.875	0.85	0.907
φ_{yy} (°)	113.4	-151.8	-66.8	18.6

FIGURE 5. Co-polarized transmission phases and amplitudes of the four selected cells. (a) Transmission phase of x-polarization. (b) Transmission amplitude of x-polarization. (c) Transmission phase of y-polarization. (d) Transmission amplitude of y-polarization.
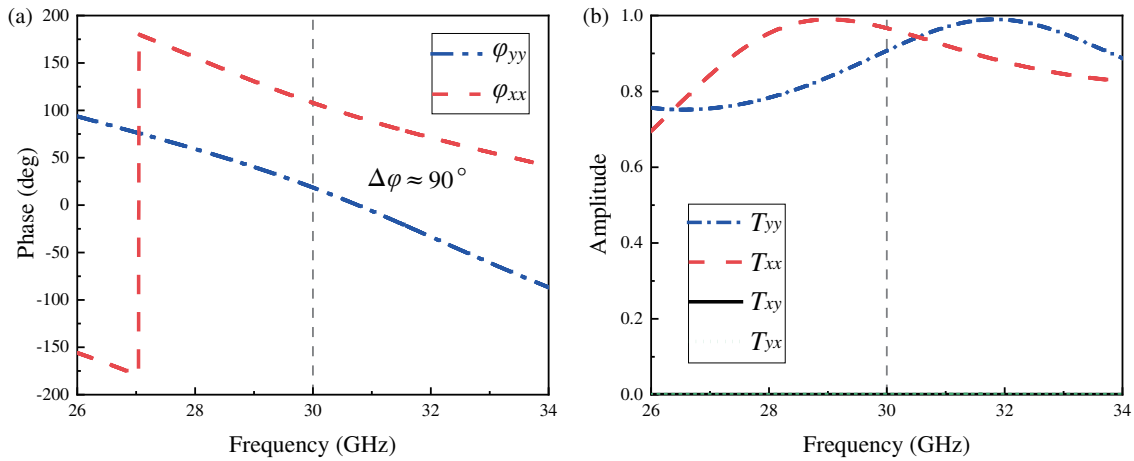
FIGURE 6. Transmissive amplitude and phase response of cell 4. (a) Transmissive phase. (b) Transmissive amplitude.

taining a 90° phase difference between each cell's x- and y-polarizations.

Taking cell 4 as an example, Fig. 6 shows the simulation results derived from simultaneously incident x- and y-polarized waves in the electromagnetic simulation software CST. The phase difference $\Delta\varphi$ between the co-polarized transmitted phases φ_{xx} and φ_{yy} is kept in the range of 90°. Furthermore, at the center frequency of 30 GHz, the co-polarized transmission amplitudes T_{xx} and T_{yy} are both greater than 0.9, while the cross-polarized transmission amplitudes T_{xy} and T_{yx} are close to 0 indicating that there is almost no interconversion between the LP components. The next three cells' amplitude and phase responses are essentially the same as those of cell 4, and all of them can efficiently convert from line to circular polarization.

3. DESIGN AND SIMULATION OF METASURFACE ARRAYS

The electric field distribution required to generate multiple beams via Transmission Array (TA) can be obtained by superposing each beam's field distribution, and then the dimensions of each unit are arranged based on the calculation results. The electric field distribution of a metasurface array capable of generating N beams can be described as [14]:

$$E(x_i, y_j) = \sum_{n=1}^{N} A_n(x_i, y_j) \exp(-j\phi_n(x_i, y_j)) \quad (3)$$

where (x_i, y_j) denotes the center position of the ith row and jth column of the unit cell, and $A_n(x_i, y_j)$ and $\phi_n(x_i, y_j)$ denote the amplitude and phase that each unit needs to be supplied to form the nth beam. By adjusting the magnitude of $A_n(x_i, y_j)$, beams with different gains can be obtained. Assuming that the metasurface array is illuminated vertically by a feed source at a distance of F, the necessary phase compensation for the n-th beam transmitting at an angle (θ_n, φ_n) is:

$$\phi_n(x_i, y_j) = \left[\left(\sqrt{(x_i - x_0)^2 + (y_i - y_0)^2 + F^2} - F \right) \right.$$

$$\left. + (x_i \sin\theta_n \cos\varphi_n + y_j \sin\theta_n \sin\varphi_n) \right] \frac{2\pi}{\lambda_0} \quad (4)$$

where λ_0 is the operating wavelength in free space, and (x_0, y_0) is the coordinate of the center position of the metasurface array. We set the expected radiation threebeam angles (θ_n, φ_n) as $(30°, 90°)$, $(30°, 210°)$, and $(30°, 330°)$, and set F as 60 mm, and $A_n = 1$ ($n = 1, 2, 3$). The array consists of 40×40 cells with a size of 124 mm $\times$ 124 mm, and the phase distribution of the metasurface array can be calculated according to Eqs. (3) and (4), as depicted in Fig. 7(a). By deploying the chosen four discrete units, the final CP multibeam metasurface array can be obtained, as illustrated in Fig. 7(b).

In this research, a linearly polarized patch antenna is designed as a feed source for joint simulation with the metasurface array, as described in Fig. 8. The dielectric substrate material of the patch antenna is F4B with a thickness of 0.4 mm, a relative permittivity of 2.2 (tan $\delta = 0.001$), a side length of the dielectric substrate and the metal floor of $p = 6$ mm, and a circular metal patch radius of $r = 1.76$ mm. The patch antenna is fed by a coaxial cable, and the feed point is $x_f = 0.6$ mm from the center of the circular patch. The far-field radiation direction pattern shows good agreement in both the xoz and yoz planes. At the center frequency of 30 GHz, the antenna's $|S_{11}|$ is less than -30 dB, and the realized gain approaches 7.3 dBi. The frequency range where the reflection coefficient $|S_{11}|$ of the feed antenna is less than -10 dB is 29.1 GHz to 30.9 GHz which meets the feed antenna's performance needs.

The phase center of the feed antenna is set at $F = 60$ mm, directly below the center of the metasurface array for the joint simulation. By rotating the patch antenna around the z-axis, the incident wave's polarization can be changed. As seen in Fig. 9, the LP wave radiated from the feed source can be converted into three RHCP beams when the incident wave's polarization direction is 45°. The three beams have transmission angles (θ, φ) of $(30°, 90°)$, $(30°, 210°)$, and $(30°, 330°)$.

The two-dimensional realized gain and AR of the metasurface are shown in Fig. 10. Three beams at the center frequency of 30 GHz have realized gains of 20.9 dBi, 20.7 dBi,
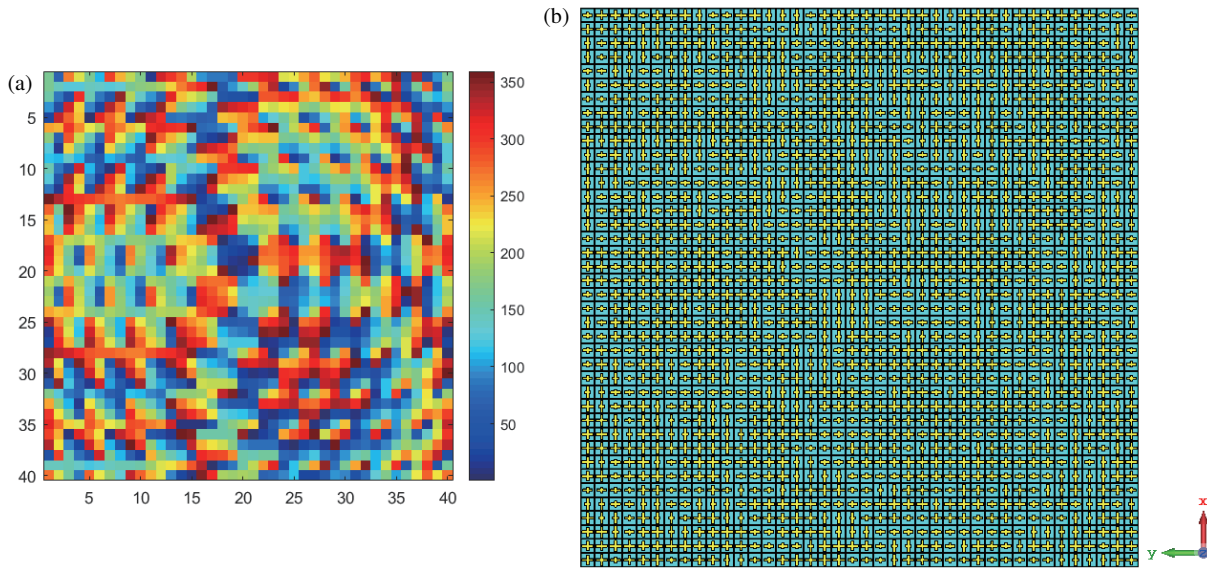
FIGURE 7. Design of a CP three-beam metasurface of equal-gain. (a) Phase distribution. (b) Metasurface array.
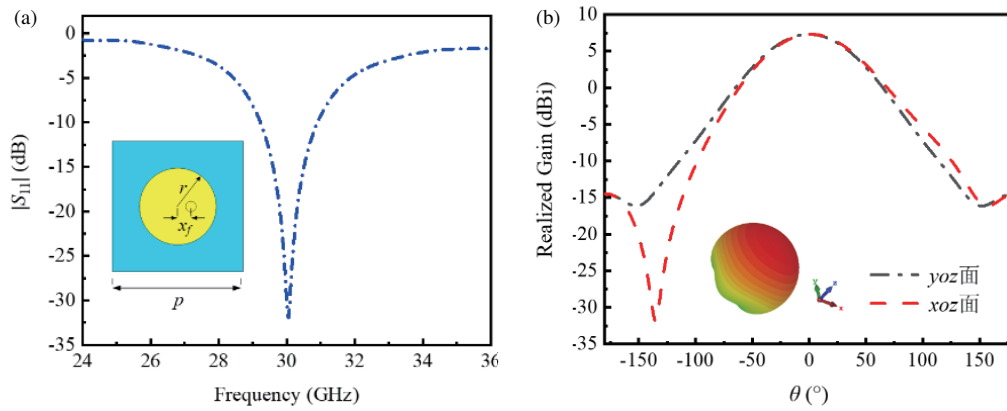

FIGURE 8. Structure of the feed source antenna and simulation results. (a) The structure of the feed source antenna and $|S_{11}|$. (b) Far-field pattern and realized gain of the feed source antenna.
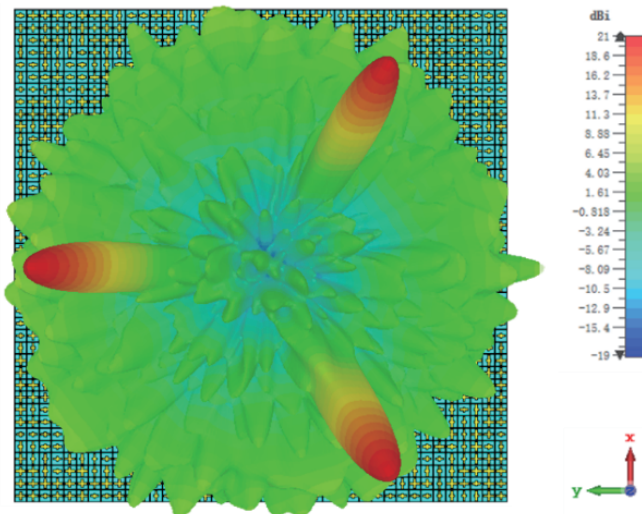

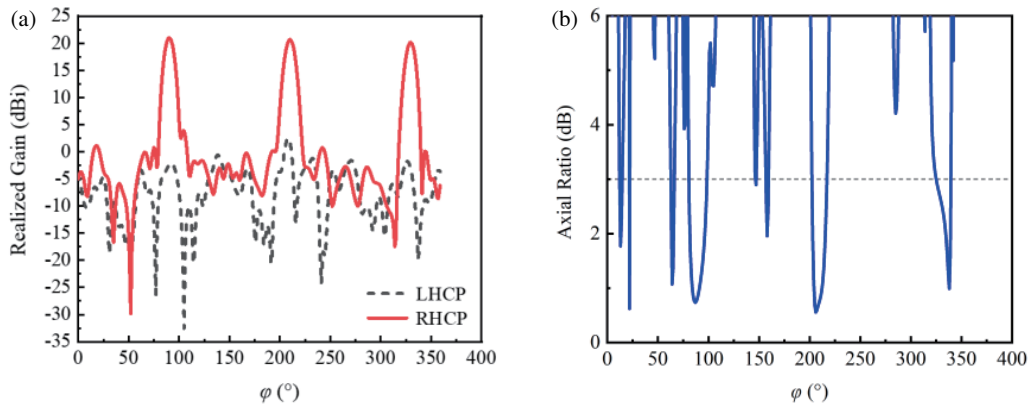**FIGURE 9**. 3D far-field radiation direction pattern for 45° LP wave incidence.

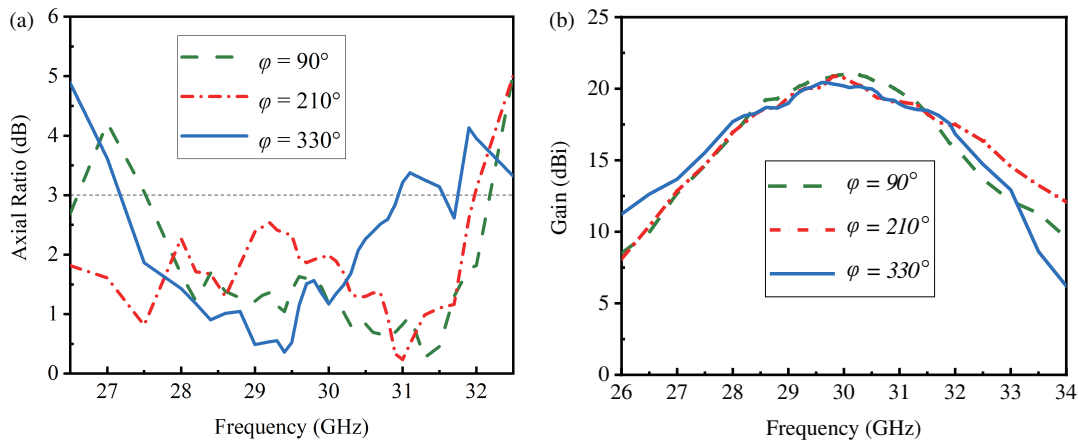FIGURE 10. Gain and AR of three beams at 30 GHz ($\theta = 30°$). (a) Gain. (b) Axial ratio.

FIGURE 11. AR and gain in the center direction of three beams ($\theta = 30°$). (a) AR vs. frequency. (b) Gain vs. frequency.
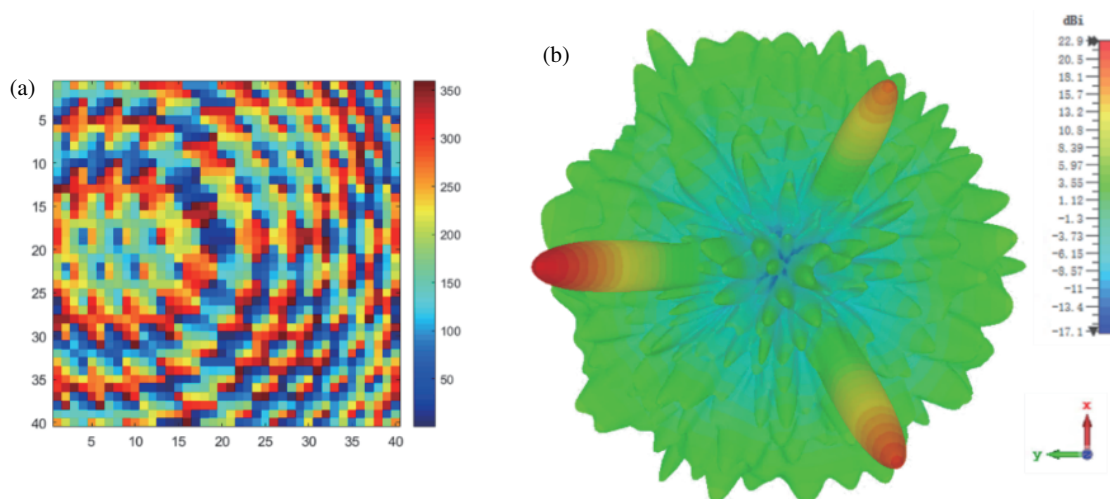

FIGURE 12. Design and simulation of a CP threebeam metasurface with unequal gain. (a) Phase distribution. (b) 3D far-field radiation pattern.

and 20.2 dBi, respectively, and the axial ratios are 1.18 dB, 1.98 dB, and 1.17 dB. A joint simulation was conducted on the metasurface array and LP patch antenna in the Ka-band, and the curves between the AR and the realized gain with frequency were obtained, as illustrated in Fig. 11. The frequency range of AR less than 3 dB is 27.6 GHz to 30.9 GHz, and the 1 dB realized gain frequency range is 29.1 dBi to 30.9 dBi. Combined with $|S_{11}|$ of the feed antenna in Fig. 8(a), the overlapped
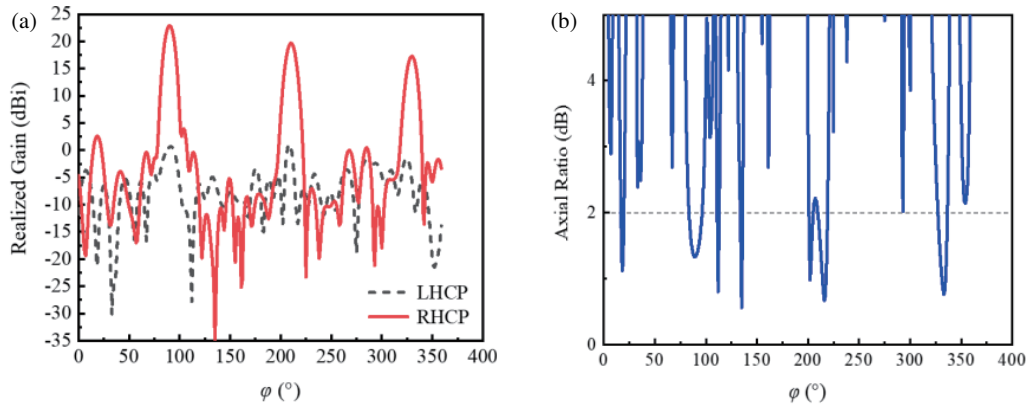
FIGURE 13. Gain and AR of the unequal gain metasurface at 30 GHz ($\theta = 30°$). (a) Gain of three beams. (b) AR of three beams.

TABLE 2. Comparison of this work with other designs.

Ref	Freq (GHz)	Types	Beams	3-dB AR BW	Gain (dBi)	Gain ratio
[15]	28	Resonant	1	83%	NA	NA
[16]	15	Geometric	2	0.7%	14.5	1 : 1
[17]	13	Resonant	4	9.1%	8.27	1 : 1 : 1 : 1
This work	30	Resonant	3	6%	22.9/19.7/17.3	1 : 0.86 : 0.76

bandwidth of the 3 dB axial ratio and 1 dB realized gain with $|S_{11}|$ is 29.1 GHz to 30.9 GHz, i.e., the relative bandwidth is 6% (1.8 GHz). The proposed equal-gain three-beam metasurface can achieve LCPC and multiple beams over a wide frequency range in the Ka-band.

Set the expected radiation three-beam angles (θ_n, φ_n) still as (30°, 90°) (30°, 210°), and (30°, 330°), set F to 60 mm, and the ratios of the amplitudes of the three beams are $A_1 : A_2 : A_3 = 1 : 0.9 : 0.8$. The array is made up of 40×40 cells, with a size of 124 mm $\times$ 124 mm. Using Eqs. (3) and (4), it is easy to obtain the phase distribution pattern of the unequal-gain metasurface array, which is displayed in Fig. 12(a). The 3D far-field radiation pattern obtained with CST is depicted in Fig. 12(b). It can be seen from Fig. 13 that at 30 GHz, the three beams' center directional AR values are 1.33 dB, 1.93 dB, and 1.21 dB, all less than 2 dB. The gain values are 22.9 dBi, 19.7 dBi, and 17.3 dBi, respectively, resulting in a gain ratio around 1 : 0.86 : 0.76, which is basically consistent with the theoretical values.

We compared this paper to other similar designs, as indicated in Table 2. Ref. [15] obtained a wide 3 dB axial ratio bandwidth that covered the K/Ka band of satellite communication. Ref. [16] realized the symmetric transmission of dual CP beams using the principle that LP waves can be decomposed into two CP waves with opposing rotation orientations. Ref. [17] proposes a Ku-band four-beam CP metasurface that converts LP waves into CP waves by exciting four ports. However, the LCPC metasurfaces with multi-beam presented in this paper have good axial ratio performance and high gain characteristics in the broadband range of the Ka-band, as well as the ability to achieve an adjustable gain ratio. It can effectively reduce

multipath fading and atmospheric influences and has promising applications in satellite communication systems.

4. CONCLUSION

Circularly polarized multi-beam metasurfaces with equal and unequal gains in the Ka-band are proposed in this paper. The metasurface unit is composed of a metal square ring and a cross-shaped structure. The phase of the x- and y-polarized waves can be controlled independently by changing the transverse and longitudinal arm lengths of the cross-shaped structure, resulting in 350° phase coverage. Choose four discrete elements that satisfy the requirements for LCPC as candidate elements, and then arrange the unit cell following the multi-beam superposition theory with an array size of 124 mm$\times$124 mm. The simulation results reveal that the metasurface can convert incident LP waves to RHCP waves and transmit three beams with equal or unequal gain at an angle preset. Circular polarization and multi-beam electromagnetic wave transmission may successfully resist atmospheric effects and multipath fading in satellite communication, enhance spectrum utilization efficiency and anti-interference capability, provide dependable support for flexible point-to-multipoint communication transmission and wide area coverage, and promote satellite communication technology.

REFERENCES

[1] You, L., K. X. Li, J. Wang, X. Gao, X. G. Xia, and B. Ottersten, "Massive MIMO transmission for LEO satellite communications," *IEEE Journal on Selected Areas in Communications*, Vol. 38, No. 8, 1851–1865, 2020.

[2] Yang, J., S. T. Chen, M. Chen, J. C. Ke, M. Z. Chen, C. Zhang, R. Yang, X. Li, Q. Cheng, and T. J. Cui, "Folded transmitarray antenna with circular polarization based on metasurface," *IEEE Transactions on Antennas and Propagation*, Vol. 69, No. 2, 806–814, 2020.

[3] Takahashi, M., Y. Kawamoto, N. Kato, A. Miura, and M. Toyoshima, "Adaptive power resource allocation with multi-beam directivity control in high-throughput satellite communication systems," *IEEE Wireless Communications Letters*, Vol. 8, No. 4, 1248–1251, 2019.

[4] Mysore, B. S., E. Lagunas, S. Chatzinotas, and B. Ottersten, "Precoding for satellite communications: Why, how and what next?" *IEEE Communications Letters*, Vol. 25, No. 8, 2453–2457, 2021.

[5] Abdelrahman, A. H., P. Nayeri, A. Z. Elsherbeni, and F. Yang, "Single-feed quad-beam transmitarray antenna design," *IEEE Transactions on Antennas and Propagation*, Vol. 64, No. 3, 953–959, 2016.

[6] Ma, X., Y. Liao, H. Huang, and W. Zhang, "A dual-band circular polarization waveguide slot antenna for 5G communication," *IEEE Antennas and Wireless Propagation Letters*, Vol. 19, No. 3, 340–344, 2020.

[7] Shao-He, L., J.-S. Li, and J.-Z. Sun, "Terahertz wave front manipulation based on pancharatnam-berry coding metasurface," *Optical Materials Express*, Vol. 9, No. 3, 1118–1127, 2019.

[8] Bao, L., R. Y. Wu, X. Fu, Q. Ma, G. D. Bai, J. Mu, R. Jiang, and T. J. Cui, "Multi-beam forming and controls by metasurface with phase and amplitude modulations," *IEEE Transactions on Antennas and Propagation*, Vol. 67, No. 10, 6680–6685, 2019.

[9] Sun, Q., Y.-L. Ban, X.-F. Li, J. Hu, and Z. Nie, "A passive metasurface for gain enhancement of wide-angle millimeter-wave multibeam array antenna," *IEEE Antennas and Wireless Propagation Letters*, Vol. 22, No. 6, 1316–1320, 2023.

[10] Wang, H. B., Y. J. Cheng, and Z. N. Chen, "Dual-band miniaturized linear-to-circular metasurface polarization converter with wideband and wide-angle axial ratio," *IEEE Transactions on Antennas and Propagation*, Vol. 69, No. 12, 9021–9025, 2021.

[11] Chandra, M., S. K. Ghosh, M. Thottappan, and S. Bhattacharyya, "A transmittive-type metasurface for dual-band linear to circular polarization conversion," in *2022 IEEE Microwaves, Antennas, and Propagation Conference (MAPCON)*, 1674–1679, 2022.

[12] Yang, W., K. Chen, Y. Zheng, K. Tang, J. Zhao, and Y. Feng, "Compact multibeam metasurface lens antenna with circular polarization for 5G millimeter-wave application," in *2021 13th Global Symposium on Millimeter-waves & Terahertz (GSMM)*, 1–3, Nanjing, China, 2021.

[13] Jiang, Z. H., L. Kang, T. Yue, W. Hong, and D. H. Werner, "Wideband transmit arrays based on anisotropic impedance surfaces for circularly polarized single-feed multibeam generation in the Q-band," *IEEE Transactions on Antennas and Propagation*, Vol. 68, No. 1, 217–229, 2019.

[14] Liu, X., Z. Yan, E. Wang, X. Zhao, T. Zhang, and F. Fan, "Multibeam forming with arbitrary radiation power ratios based on a conformal amplitude — phase-controlled metasurface," *IEEE Transactions on Antennas and Propagation*, Vol. 71, No. 4, 3707–3712, 2023.

[15] Shukoor, M. A., M. P. Reddy, and S. Dey, "Novel wideband single-layered substrate linear-to-circular metasurface enabled transmission type polarizer for K-/Ka-bands satellite applications," in *2022 Asia-pacific Microwave Conference (APMC)*, 88–90, Yokohama, Japan, 2022.

[16] Yang, P., R. Yang, and Y. Li, "Dual circularly polarized split beam generation by a metasurface sandwich-based Fabry-Perot resonator antenna in Ku-band," *IEEE Antennas and Wireless Propagation Letters*, Vol. 20, No. 6, 933–937, 2021.

[17] Liu, Q., M.-Y. Xia, and W.-M. Zhang, "A compact circularly polarized multibeam antenna using defected polarization conversion metasurface," *IEEE Antennas and Wireless Propagation Letters*, Vol. 22, No. 8, 1892–1896, 2023.